A predicted binding site for cholesterol on the GABAA receptor.

Jérôme Hénin, Reza Salari, Sruthi Murlidaran, Grace Brannigan

A Predicted Binding Site for Cholesterol on the $GABA_A$ Receptor

Jérôme Hénin,[†] Reza Salari,[‡§] Sruthi Murlidaran,[§] and Grace Brannigan[‡§*]
[†]Laboratoire de Biochimie Théorique, CNRS, IBPC, and Université Paris Diderot, Paris, France; [‡]Department of Physics and [§]Center for Computational and Integrative Biology, Rutgers University-Camden, Camden, New Jersey

ABSTRACT Modulation of the GABA type A receptor ($GABA_AR$) function by cholesterol and other steroids is documented at the functional level, yet its structural basis is largely unknown. Current data on structurally related modulators suggest that cholesterol binds to subunit interfaces between transmembrane domains of the $GABA_AR$. We construct homology models of a human $GABA_AR$ based on the structure of the glutamate-gated chloride channel GluCl of *Caenorhabditis elegans*. The models show the possibility of previously unreported disulfide bridges linking the M1 and M3 transmembrane helices in the α and γ subunits. We discuss the biological relevance of such disulfide bridges. Using our models, we investigate cholesterol binding to intersubunit cavities of the $GABA_AR$ transmembrane domain. We find that very similar binding modes are predicted independently by three approaches: analogy with ivermectin in the GluCl crystal structure, automated docking by AutoDock, and spontaneous rebinding events in unbiased molecular dynamics simulations. Taken together, the models and atomistic simulations suggest a somewhat flexible binding mode, with several possible orientations. Finally, we explore the possibility that cholesterol promotes pore opening through a wedge mechanism.

INTRODUCTION

Rapid inhibition in the vertebrate central nervous system is mediated largely by the neurotransmitter γ-aminobutyric acid (GABA) acting on the GABA type A ($GABA_AR$), a Cl^- channel in the Cys-loop superfamily of ionotropic receptors (1–3). Dysfunctional $GABA_ARs$ have been implicated in multiple human diseases, including epilepsy (4), schizophrenia (5–7), Alzheimer's disease (8), and alcohol dependence (9,10). Drugs treating these disorders, as well as multiple classes of anesthetics (11–13) and sedatives (14,15) target the $GABA_AR$. In addition, $GABA_ARs$ are also modulated by endogenous cholesterol derivatives called neurosteroids (16–18), which function as natural sedatives, anesthetics, painkillers, anticonvulsants, and antianxiety agents (19).

The mechanisms through which both endogenous and exogenous lipophilic modulators exert their effects on the $GABA_AR$ have not been conclusively determined. Elucidating these mechanisms has proven challenging, in part due to lack of information regarding the structure and dynamics of the $GABA_AR$ in the absence of these modulators. No high-resolution crystal structures of the $GABA_AR$ have been published; however, a general understanding of Cys-loop receptor structure has emerged over the past decade thanks to the publication of cryoelectron microscopy (cryo-EM) images at medium resolution (20,21) obtained for a cationic homolog (the nicotinic acetylcholine receptor (nAChR)) and, more recently, high-resolution crystal structures of prokaryotic cationic members of the family, *Dickeya dadantii* and *Gloeobacter violaceus* ligand-gated ion channels (ELIC (22,23) and GLIC (24–28), respectively).

From these and earlier studies, it is known that ion channels in this family are pentamers, with five subunits arranged around a central pore; consequently, they are often called pentameric ligand-gated ion channels (pLGICs) (29). It has also been shown that each subunit has an extracellular domain composed of β sandwiches and a transmembrane domain composed of a four-helix bundle, with helices labeled M1–M4. Some pLGICs also have a long intracellular domain of unknown structure; in nAChRs, this domain has been shown (30) to be unnecessary for function. Neurotransmitters bind to sites at subunit interfaces in the extracellular domain, and the signal is transmitted to the pore through a poorly understood mechanism (31).

Only one high-resolution structure for either a eukaryotic or anion-selective member of the family has been published (32): the glutamate-gated chloride channel (GluCl) from *Caenorhabditis elegans* has been crystallized in the open state in the presence of a lipophilic agonist (ivermectin) bound to the subunit interface in the transmembrane domain, and in both the presence and absence of its neurotransmitter, glutamate. The conformation of the structure in the absence of ivermectin is unknown. Based on the orientation of ivermectin in those crystal structures, Hibbs and Gouaux proposed that hydrogen bonding to M2 serine 15′ is essential for potentiation and activation and suggested that activation by ivermectin proceeded due to a wedge mechanism in which the agonist increases the radius of the ring formed by the M1 and M3 helices, thus causing the inner ring, composed of pore-lining M2 helices, to expand. It was then proposed that hydrogen bonding with Ser15′ on M2 stabilizes the open state of the receptor. However, such hydrogen bonds are not always conserved in other Cys-loop receptors that are highly sensitive to ivermectin, leading Lynagh and Lynch (33) to

Submitted December 6, 2013, and accepted for publication March 14, 2014.

*Correspondence: Grace.Brannigan@rutgers.edu

Editor: Carmen Domene.

0006-3495/14/05/1938/12 $2.00

http://dx.doi.org/10.1016/j.bpj.2014.03.024

suggest that hydrogen bonding may be a secondary effect of the mechanism.

Since ivermectin potentiates both GluCl and the $GABA_AR$ in a similar manner, the modes of interaction can be expected to be similar as well. On a structural level, the ivermectin site in GluCl forms a cavity that transfers to GluCl-based models of $GABA_ARs$. All available crystal structures of GluCl have the agonist ivermectin bound to intersubunit sites in the transmembrane domain, but relaxation in the absence of bound ivermectin has been explored in two recent computational studies (34,35). In these studies, the empty site did not fill with water but saw a reduction in volume due to local changes in protein structure, whereas the remaining cavity was filled with phospholipid chains from the bilayer. We note that binding to the vacant site of other lipophilic molecules, such as cholesterol, was excluded from potential observation because both model bilayers were made of pure phospholipid.

Still, numerous studies have indicated the existence of specific interactions between eukaryotic pLGICs and cholesterol, which is abundant in synaptic membranes (36). Interactions of the nAChR with cholesterol have been extensively studied (37–47) due to an early observation of a functional requirement after purification and reconstitution; in such systems, addition of cholesterol to a reconstitution mixture can confer up to a fivefold gain of function. However, a significant obstacle to quantifying effects of cholesterol experimentally lies in the difficulties in controlling the amount and distribution of cholesterol in the membrane-protein system.

Some later experiments, however, depleted the native membranes of cholesterol using liposomes (42,48,49) or cyclodextrins (50–52); as indicated by the result that some cholesterol (~36 molecules/receptor) remains in the system despite extensive depletion (42), this procedure likely primarily modulates the cholesterol content of the bulk membrane. In a recent study, it was reported that the nAChR reconstituted in bilayers free of cholesterol but of sufficient thickness undergoes conformational transitions on a slow timescale (minutes to hours) (53). Although those experiments indicate a role for hydrophobic thickness in nAChR modulation, they do not conclude that the nAChR can be fully functional in the absence of cholesterol.

Simulation studies (54,55) have investigated interactions between membrane cholesterol and the nAChR, although timescales were likely insufficient to achieve mixing equilibrium. After the publication of an atomic cryo-EM structure for the nAChR (20,21) exhibiting significant gaps in transmembrane protein density, we proposed (54) that cholesterol could occupy deeply buried (nonannular) sites, and we demonstrated that models containing significant amounts of embedded cholesterol were the most stable under molecular dynamics (MD) simulation.

Interactions of the $GABA_A$ with cholesterol have received less attention, although purification and reconstitution protocols for $GABA_ARs$ either include cholesterol (56,57) or yield nonfunctional and unstable receptors (56). Sooksawate and Simmonds reported that coexisting indirect and direct mechanisms account for cholesterol modulation of the $GABA_AR$ (58); in this system, both enrichment and depletion of cholesterol reduce the potency of the receptor, but although the enrichment effect can be reproduced using epicholesterol, the depletion effect cannot be reversed by introducing epicholesterol. The authors hypothesize that the depletion effect reflects direct interactions, whereas the enrichment effect is mediated by physical properties of the membrane. Consequently, due in part to the challenges inherent in controlling the amount or distribution of cholesterol even in the experimental control systems, a simple functional effect of directly bound cholesterol on $GABA_ARs$ has not been identified.

The presence of specific interactions of cholesterol with $GABA_ARs$ is further suggested by the observation that such receptors can be positively modulated, and even activated, by cholesterol derivatives known as neurosteroids (16–18). Two examples of potent, naturally occurring $GABA_A$-active steroids are 3α-hydroxy-5α-pregnan-20-one (allopregnanolone) and 5α-pregnane-3α,21-diol-20-one (THDOC). Positive Modulation by neurosteroids requires a hydroxyl at C3, as in cholesterol, but also requires a hydrogen-bond-accepting group at C20 (usually a ketone) (19,59,60). The interface between α and β subunits in the transmembrane domain of the $GABA_AR$, in the same region as the ivermectin site in GluCl, has been identified through mutagenesis as the likely site of activation by the positively modulating neurosteroids allopregnanolone and THDOC (61,62), although this interpretation may depend on the structural model considered (63). The mechanism through which the different functional group at C20 allows the neurosteroid to activate the receptors (in contrast to cholesterol, which does not cause activation) has not been determined. Modulation by neurosteroids is, however, dependent on cholesterol concentration (64). Furthermore, the antagonistic effect upon cholesterol enrichment is selective of cholesterol versus epicholesterol (58) and may therefore be ascribed to specific cholesterol binding, possibly competitive binding to the intersubunit sites.

Finally, some degree of pharmacological similarity between ivermectin and steroids at the $GABA_A$ transmembrane domain is expected. Ivermectin is known to bind to $GABA_ARs$ and potentiate their response to GABA or even activate the receptors in the absence of GABA (65–67). A binding site for cholesterol at the subunit interface also forming the neurosteroid site would consequently be consistent with the available data.

In this report, we explore potential specific interactions between cholesterol and the intersubunit (ivermectin) sites on several different models of an $\alpha_1\beta_1\gamma_2$ $GABA_A$ receptor. We find that docking calculations do place cholesterol in the intersubunit sites. Using MD simulation, we explore the

dynamic behavior of bound cholesterol molecules, as well as its short-time effects on transmembrane domain conformation. In particular, we test whether such cholesterol acts as a nonspecific wedge on the ring of M1 and M3 helices.

METHODS

Homology modeling

No high-resolution structure of a $GABA_AR$ is presently available, but multiple structures for members of the pLGIC superfamily have been published; for simulations of the $GABA_AR$, we must rely on homology models built on these templates. Such modeling is supported by two properties of pLGICs:

1. Alignments for the pLGIC superfamily are robust: large multiple alignments have been constructed using sophisticated methods for detecting remote homology (68,69) and confirmed by structural alignment in the cases where structures are available (ELIC, GLIC, and GluCl). Furthermore, accuracy of the calculations for this manuscript depend largely on the resolution of the structure in the transmembrane domain, for which the alignment between $GABA_AR$ and the template, GluCl, is essentially unambiguous and has no gaps.
2. All existing structures indicate a tightly conserved fold for the pLGIC superfamily, particularly in the transmembrane domain. Despite the evolutionary distance (24% overall sequence identity) between GluCl and GLIC, the protein backbones show remarkable overlap. In our case, the model and template are likely even more similar: GluCl and $GABA_AR$ (both anionic, eukaryotic, and ligand-gated) exhibit 32% sequence identity overall, and 46% identity in the transmembrane domain.

Other groups have found available templates and alignments to yield models of $GABA_ARs$ robust enough for pharmacological studies (70,71). We built homology models using GluCl (PDB code 3RHW) as a template and the alignments published with that structure. The standard procedure for oligomer modeling in MODELLER (72) was used to build 40 human $\alpha_1\beta_1\gamma_2$ $GABA_AR$ homology models from the template and alignments, with disulfide bridges specified in the α and γ transmembrane domains. Stereochemistry was checked using the Chirality plugin (73) in VMD (74), and the model with the lowest score was chosen for further simulation (Model 1). To conservatively estimate the uncertainty in results due to the use of a homology model with underdetermined side chains, a second intermediate-scoring model (Model 2) that displayed an alternate pattern of salt bridging in the transmembrane domain, including fivefold symmetry for the salt bridges in the extracellular half of the transmembrane domain (αM2:Arg274-M3:Asp287, βM2:Asp282-M3:Lys279, γM2:Arg284-M3:Asp297), was also selected for simulation. To test for the influence of modeling details on cholesterol-protein interactions, another alternate model (Model 3) was constructed by further optimizing side chains using the program SCWRL4 (75); orientation of polar side chains was then corrected to optimize the hydrogen-bond network using MolProbity (76).

Cholesterol docking

A first set of starting coordinates for bound cholesterol was generated by analogy with ivermectin. The cyclohexanol ring of cholesterol was aligned with the benzofuran moiety of ivermectin bound to the template, as shown in Fig. S3; these poses retained the symmetry of the GluCl template, and were not affected by pseudosymmetry of the $GABA_AR$. These coordinates were the initial conditions for simulations of Model 1 and Model 2.

Docking of cholesterol molecules to Model 3 was performed in a completely independent manner: automated docking was performed by the AutoDock Vina software package (77). Input files were prepared using the University of California, San Francisco's Chimera (78). All docking attempts on search spaces including the hydrophobic pore returned binding poses in the pore, which are physiologically unrealistic. For that reason, the pore itself was excluded from all production runs. In a first docking calculation, the cholesterol was flexible, whereas the protein was rigid, and the search space included the complete transmembrane domain. A second stage sought to refine the search in the β_1-α_1 and β_1-γ_2 interfaces; in these searches, two protein residues whose side chains were protruding into the intersubunit space were made flexible (β_1, M227 and L231). Together, these searches produced a generally similar set of poses for cholesterol in all five intersubunit clefts. To account for the absence of a lipid bilayer in docking calculations, poses involving significant interactions with membrane-facing residues were excluded, assuming that cholesterol in such poses could be displaced by phospholipids; deeply bound poses were favored. In a similar way, reverse poses where the cholesterol hydroxyl was located outside the pocket were excluded. After applying these criteria, there remained at least one high-scoring pose for each site (within two score units of the maximum): the best-scoring pose for each interface was selected for further modeling.

Solvated simulation systems

The proteins with bound cholesterol and without cholesterol were both placed in a lipid bilayer composed of 4:1 phosphatidylcholine (POPC)/cholesterol mixture, generated using the CHARMM-GUI Membrane builder (79) to build a patch of 72 POPC molecules and 18 cholesterol molecules, and then duplicating the patch three times in Visual Molecular Dynamics (VMD). The cholesterol concentration of 20% is in the lower part of the physiological range (36). This ensures a realistic bilayer structure, without running the risk of biasing cholesterol-protein interactions toward excessive binding through a high cholesterol concentration. The transmembrane domain of the protein (and any bound cholesterol) was aligned to the membrane and overlapping lipids were removed. The final system with bound cholesterol had 266 POPC molecules and 71 membrane cholesterol molecules, whereas the final system with no bound cholesterol had 268 POPC molecules and 71 membrane cholesterol molecules. The system was solvated using the solvate plugin of VMD, and ions were added to bring the system to a neutral 0.15 M concentration using the autoionize plugin. The total system size was ~157,000 atoms for all systems.

Simulation details

All simulations used the CHARMM22-CMAP force field with torsional corrections for proteins (80,81). The CHARMM36 (82) model was used for phospholipids, ions, and water. CHARMM36 (83) parameters were used for cholesterol in Models 1 and 2, and updated, yet very similar parameters (CHARMM36c (84)) were used for Model 3. Energy minimization and MD simulations were performed using the NAMD package versions 2.8 and 2.9 (85). All simulations employed periodic boundary conditions; long-range electrostatics were handled with the smooth particle mesh Ewald method (86), and a cutoff of 1.2 nm was used for Lennard-Jones potentials, with a switching function applied starting at 1.0 nm. All simulations were run in the NPT ensemble with weak coupling to a Langevin thermostat and barostat at a respective 300 K and 1 atm. All bonds to hydrogen atoms were constrained using the SHAKE/RATTLE algorithm. A multiple-time-step rRESPA method was used, controlled with a high-frequency time step of 2 fs and a low-frequency time step of 4 fs.

The systems were energy-minimized for 1000 steps, then simulated for 5 ns with restraints of 1 kcal/mol/Å^2 applied to the C_α atoms of the protein. Restraints were then lifted, and 195 ns of nearly unrestrained simulation was carried out. During this period of the simulation, only harmonic restraints (force constant, 0.4 kcal/mol/Å^2) between the intracellular ends of the M3 and M4 helices were used, to mimic the effects of the intracellular domain and prevent separation of the M4 helix from the rest of the bundle.

To provide an estimate for statistical error due to finite temperature, three simulations (a–c) of Model 1-Chol were run; these replicas differ only in the random seed used for the thermostat and barostat.

Structural analysis of simulated trajectories

Cholesterol orientation within the intersubunit cleft was measured along two coordinates, a tilt angle and a flip angle. Tilt is defined as the angle between the long axis of cholesterol and the membrane plane. Here, the long axis was defined as the vector joining atoms C3 and C17, at opposite ends of the steroid nucleus. The flip angle is defined as the angle between the vector joining cholesterol atoms C2 and C4 (in the β position of the hydroxyl group) and the membrane plane.

Hydrogen bonds were defined as those with an O-H separation of <3.3 Å and an angle of $<25°$. For analysis of pore profiles, snapshots were extracted every 1 ns from the simulations and were subsequently aligned. The HOLE software (87) was used to measure pore radius for each snapshot, and the resulting pore profiles were analyzed and plotted using a custom Python script. Measurements of geometric pore properties were conducted using VMD scripts (for definitions, see Fig. 5).

RESULTS

$GABA_A$ models

Three homology models of the $\alpha_1\beta_1\gamma_2$ $GABA_A$ receptor were built based on the recent crystal structure of the glutamate-gated chloride channel (GluCl) from *C. elegans* (32) (PDB code 3RHW). Several potentially essential interactions in the transmembrane domain emerged in these models. The most striking result was the existence of a potential disulfide bridge in the core of the transmembrane domain, in the α and γ subunits, between helices M1 and M3 (Fig. S1).

The template GluCl possesses two neighboring cysteine residues, Cys225 on M1 and Cys283 on M3. Although Cys283 faces M1, Cys225 points away from M3, so that the side chains are too distant to form a disulfide bond in GluCl (distance between C_β atoms, 7.9 Å). $GABA_AR$ subunits α and γ have a cysteine residue at the previous position in the sequence, which points directly toward M3; this brings the side chains within bonding distance in the conformation directly derived from the template. As a test, we produced alternate models wherein this disulfide bond was or was not enforced; this produced no significant changes to the modeling score. Most likely, such disulfide bridges were never envisioned because the previously available template structure (Unwin's structure of the nAChR) incorrectly assigns residues in the transmembrane domain (88), yielding homology models where the cysteines are not in contact. Such a possibility is noted only in passing in one recent report (71).

The alignment of this region is robust: for the region spanning M1–M3, there are no gaps in the multiple alignment, and the three $GABA_A$ chains have sequence identities with GluCl of 46%, 48%, and 41%, respectively. Thus, a misplacement of the cysteine residues involved due to alignment errors is very unlikely. This is confirmed by comparison with the model of an $\alpha_1\beta_1\gamma_2$ $GABA_AR$ published by Bergmann et al. (70), which places the cysteine residues at the same positions, although the authors do not comment on the possibility of disulfide bridging. Based on the alignment of various prokaryotic and eukaryotic pLGIC sequences by Tasneem et al. (68), we examined the distribution of both cysteine residues across receptor types and taxonomic groups. Interestingly, although each of the cysteines is common among eukaryotic pLGICs, this potentially bridging pair of cysteines is rare (Fig. S2). The general trend is for prokaryotic receptors to lack both cysteines, for anionic as well as 5HT3 receptors to have only the M3 cysteine, and for acetylcholine receptors to possess only the M1 cysteine, with only $GABA_A$ α and γ subunits having both. The only exceptions to these rules are a few prokaryotic and invertebrate receptors. To look for a possible functional significance of these residues, we investigated their variability more specifically among GABA receptor subunits through sequence alignments of vertebrate $GABA_A$ subunits from the Uniprot database. The pattern is conserved across subtypes and species: all annotated subunits of types α and γ possess both cysteines, whereas β subunits have the cysteine on M3 but lack that on M1. This extends to vertebrates (most of the available sequences), but also to invertebrates such as *Lymnea* and *Drosophila*. The only exception we found is a GABA receptor subunit β from *C. elegans* (Uniprot ID O18276), which has both cysteines.

This raises the distinct possibility that the presence or absence of these disulfide bridges is not neutral, but could play a specific functional role in α and γ subunits of $GABA_ARs$ at least in all vertebrate species. An argument against such a role is the fact that wild-type receptors seem functionally unaffected by exposure to the reducing agent dithiothreitol (89,90). A more in-depth investigation could involve mutagenesis, either mutating one of the bridging cysteines to serine or introducing the missing M1 cysteine in a β subunit. Some of these experiments have already been performed by Akabas and co-workers. Those authors mutated endogenous cysteines from the α subunit to prepare a Cys-light version of the receptor, as a background for cross-linking experiments (91,92). Unfortunately, those studies do not report a functional comparison of the Cys-light mutant with the wild-type.

Although the bridge is highly plausible from a geometric perspective, it is unknown whether this region of the transmembrane domain is exposed to sufficient oxidizing conditions after translation to effectively produce the disulfide. Limited water accessibility between transmembrane helices may or may not allow oxidizing agents to reach the site, although the simulations presented here do indicate that the neighboring intersubunit cavity has significant water accessibility. Furthermore, cross-linking experiments have successfully formed disulfide bridges in the transmembrane domain (89–92). In classical MD simulations, disulfide bridges are part of the model and must be specified at the beginning of the simulation. The simulations reported here do include disulfide bridges in the α and γ subunits.

The impact of disulfide bonds bridging M1 and M3 in the α and γ subunits may be assessed by comparing the local

dynamics of those cysteine residues with that of their homologous counterparts in β subunits. Across all simulations, the distance between α carbons of those bridged cysteines averages 6.4 Å, with a standard deviation of 0.3 Å, whereas the same distance calculated for the homologous pair of residues in the β subunit (S229 and C288) gives an average of 7.0 Å and a standard deviation of 0.5 Å. Thus, the presence of M1-M3 disulfide cross-links seems to have only a small effect on the interhelical distance, and cause a slight reduction in the relative dynamics of these two helices.

The transmembrane domain of the receptor contains multiple charged residues. Each subunit has an acidic residue on M3 and a basic residue on M2, on the extracellular half of the receptor transmembrane domain, as specified in Methods. These residues form interhelical salt bridges in the α and γ subunits in the model, and the bridges are stable over the course of the simulations (both with and without cholesterol). In the β subunit, the analogous residues have additional salt-bridging partners on the same helices, and the interhelical salt bridges are not present in the initial coordinates for Model 1 (nor do they form over the simulation). The interhelical salt bridges are present in the initial coordinates for β subunits in Model 2.

Predicted cholesterol binding

One set of starting coordinates for bound cholesterol was generated by analogy with GluCl-bound ivermectin (Fig. S3). To confirm in an unbiased manner the possibility that cholesterol could bind to the intersubunit cavity, automated docking calculations were performed. The docking found cholesterol binding modes for each subunit interface of the $GABA_AR$ transmembrane domain, and only in those sites (after excluding the hydrophobic pore). The docking process yielded at least one pose with high predicted affinity for each site (typically -7 to -8 kcal/mol). The five poses are strongly similar, and share major features. They all occupy the cavity that binds ivermectin in the template structure, and parts of the cholesterol structure replace well-defined parts of ivermectin, as illustrated in Fig. S4.

In agreement with our initial ivermectin-based binding model, most high-scoring poses place the cyclohexanol ring of cholesterol in the position of the six-membered ring of the benzofuran moiety of ivermectin. This places the hydroxyl group in position to form a hydrogen bond with the M2 serine 15′, thus mimicking ivermectin interaction with GluCl (32). At the other end of the steroid core, the cyclopentane ring closely matches one of the six-membered rings in the spiroketal group of ivermectin. Finally, all five optimally docked cholesterol molecules share the same orientation, with the smooth side always facing toward helix M1 of one subunit and the rough side facing toward helix M3 of the other (Fig. S4). Considering that this heteromeric $\alpha_1\beta_1\gamma_2$ receptor contains five different subunit interfaces, such a fivefold symmetric docking prediction is remarkable.

The docking poses, however, adopt a different orientation than predicted by analogy with ivermectin. Although the aligned coordinates give a mostly horizontal cholesterol (in the membrane plane), docked cholesterol molecules are more tilted (Fig. 1). The two families of poses are also flipped with respect to each other: the rough side of cholesterol faces M1 in the aligned coordinates, as opposed to M3 in the docked coordinates. Time evolution of these orientation parameters in MD simulations is described below.

Cholesterol-free systems

In the simulations without any directly bound cholesterol, phospholipid acyl chains initially enter the gaps formed by the ivermectin binding site; many are expelled from the sites as they close over the course of the simulations. Although the model bilayer does contain cholesterol, the relatively short length of the simulations compared to the likely timescales required for reorientation and binding of a rigid molecule like cholesterol preclude the observation of spontaneous cholesterol binding to empty intersubunit sites. However, in simulations starting with bound cholesterol,

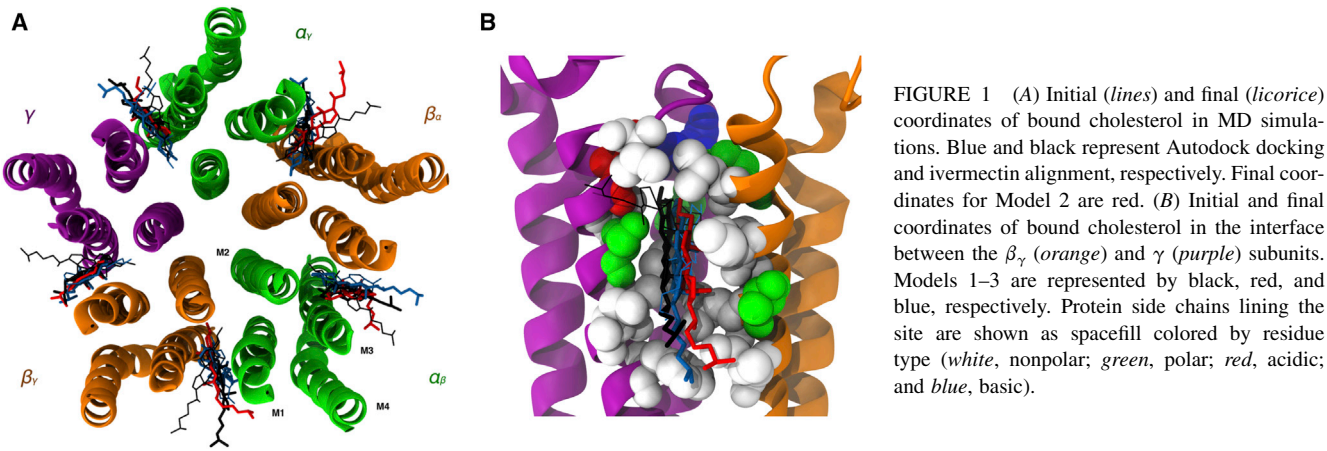

FIGURE 1 (*A*) Initial (*lines*) and final (*licorice*) coordinates of bound cholesterol in MD simulations. Blue and black represent Autodock docking and ivermectin alignment, respectively. Final coordinates for Model 2 are red. (*B*) Initial and final coordinates of bound cholesterol in the interface between the β_γ (*orange*) and γ (*purple*) subunits. Models 1–3 are represented by black, red, and blue, respectively. Protein side chains lining the site are shown as spacefill colored by residue type (*white*, nonpolar; *green*, polar; *red*, acidic; and *blue*, basic).

spontaneous unbinding and rebinding events are observed (as described below).

In both simulated models without directly bound cholesterol, the pore closes to have a minimum constriction likely too small to conduct a chloride ion, as discussed further below (Effect of cholesterol on the ion channel pore). The minimum constriction is consistently at 9′, in contrast to the minimum constriction in GluCl at −2′; since 9′ is significantly more hydrophobic, similar to the putative hydrophobic gate in the nAChR, it seems likely that a chloride ion would require a solvation shell to cross this barrier, making a slight constriction sufficient to block the passage of ions.

Dynamics of bound cholesterol

Initial coordinates from both approaches to docking cholesterol to the $GABA_AR$ are shown in Fig. 1. Average distances (projected onto the membrane plane) of the cholesterol center of masses from the pore center are shown elsewhere (see Fig. 5, *top*) Quantitative data on cholesterol fluctuations are given in Fig. S5. In general, cholesterol is seen to fluctuate within the sites, including reorientation and back-and-forth translation between the opening of the intersubunit cleft and the M2 helix that separates the cavity from the central pore.

Instances of cholesterol unbinding are observed in Models 1 and 2. In Model 2, two cholesterol molecules unbind very rapidly (within 20 ns of simulation time), presumably due to unfavorable interactions with the pocket. Perhaps surprisingly, both molecules bind again, 80–110 ns into the simulation, reaching more favorable binding modes. The process is illustrated in Fig. 2 in the case of the α_β-β_γ interface. These unexpected events provide examples of spontaneous binding of cholesterol to the intersubunit cavities, on a short timescale (<100 ns), although binding in this case is certainly facilitated by the position of cholesterol exactly at the opening, in a favorable orientation. Spontaneous binding of cholesterol from the bulk bilayer is expected to face an additional entropic barrier.

Cholesterol reorientation is measured by two angle parameters, flip, which describes rotation around the long axis, and tilt, which measures the angle formed by the long axis and the membrane plane. Time trajectories of these parameters for all simulations are represented in Fig. 3. The flip coordinate characterizes two main states: if the rough side of cholesterol faces helix M1, the angle is negative, and if it faces M3, the angle is positive. Very few flip events are observed, indicating that these states are separated by high kinetic barriers, presumably due to the asymmetric shape of the intersubunit cleft, which disfavors horizontal orientations of the cholesterol nucleus. One instance of flip (Model 2, α_β-β_γ) sidesteps this barrier by unbinding, flipping while outside the cavity, then rebinding (Fig. 3). Such a slow flip motion is reminiscent of the experimental characterization by electron paramagnetic resonance of nAChR-rich membranes, which found that in such membranes the steroid androstanol experienced hindered rotation around its long axis, with a rotation time >50 ns (93). The most likely explanation for such hindered rotation is tight binding such as that

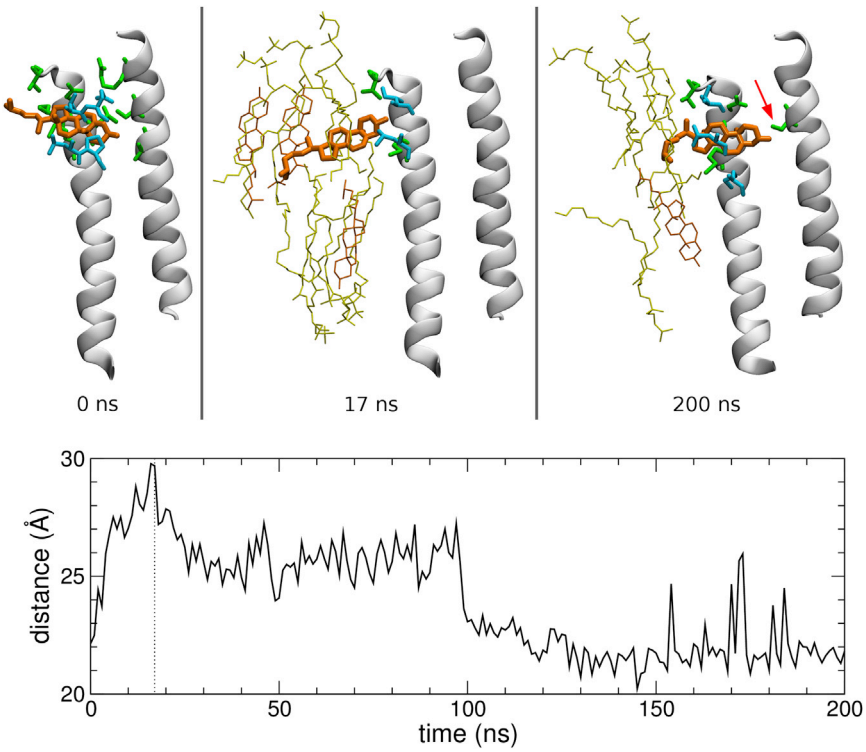

FIGURE 2 Spontaneous unbinding and rebinding event in an MD simulation. In the inital model (*upper left*), cholesterol (*orange*) is bound between helices β_γ M2-M3 (*white cartoon*) and α_β M1 (not shown). At 17 ns (*upper middle*), cholesterol has entirely exited the site and is solvated by the lipid bilayer (*lower*, *dotted line*). At 200 ns (*upper right*), it is again deeply bound at the interface, and forming a hydrogen bond with M2 serine 15′ (*red arrow*). Protein and lipid residues in contact with cholesterol in each frame are depicted as licorice (*yellow*, phospholipid; *orange*, cholesterol; *cyan*, α_β M1; *green*, β_γ M2-M3). (*Lower*) Distance between cholesterol center of mass and center of the receptor as a function of time.

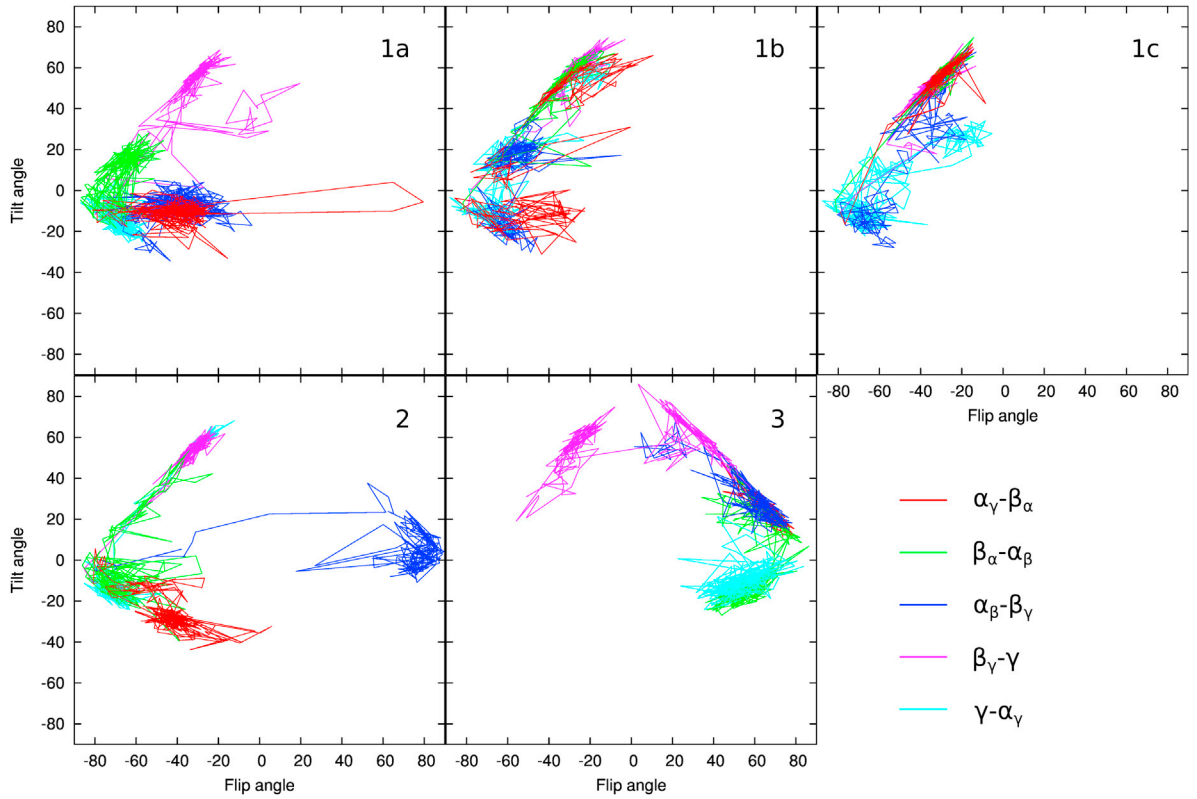

FIGURE 3 Reorientation of bound cholesterol molecules in five separate MD simulations. Each interface is color-coded (see key). The lines connect successive values of the tilt and flip angles for each bound cholesterol molecule. Tilt describes the angle between the cholesterol long axis and the membrane plane, whereas flip reflects the orientation of an axis orthogonal to the former, in the plane of the sterol nucleus. Simulations of models 1a–1c and 2 start from (−80, −11), whereas initial conditions for model 3 are in the range (50–65,10–35).

proposed here for the $GABA_AR$ and in our previous article for the nAChR (54).

Protein residues interacting with cholesterol

Receptor residues found in frequent contact with bound cholesterol in all models simulated are listed in Table 1. Note that the residues are mutually homologous, in accordance with the overall pentameric pseudosymmetry of the observed binding modes. Based on the ivermectin analogy, the key residue expected to interact with cholesterol is serine 15′ on helix M2. This interaction is described in detail in the next section. At each interface, residues belonging to helices M1 and M3 of the two subunits form a belt of nonpolar contacts around the steroid nucleus of cholesterol (Fig. 1). These residues are almost exclusively hydrophobic, with the exception of γ_2 S301.

TABLE 1 Residues forming frequent contacts with bound cholesterol

	α_1	β_1	γ_2
M1	I228	L223	I238
	L232	M227	I242
	M236	L231	L246
M2	S270	S265	S280
M3	A291	M286	S301
	Y294	F289	F304

Hydrogen bonding of cholesterol to M2 serine 15′

The role of hydrogen bonding of a pLGIC modulator to a serine residue on the M2 helix has been discussed in the case of potentiation of GluCl by ivermectin, based on crystallography (32) and site-directed mutagenesis (94,95). Examination of a broader range of pLGICs, however, indicates that presence of a serine residue at this location is not essential for ivermectin sensitivity (96). Most directly bound cholesterol molecules do form a hydrogen bond with Ser15′, as illustrated in Fig. 2.

In the simulations presented here, serine residues at the M2 15′ position in all α and β subunits are found to form H-bonds to bound cholesterol for at least 80% of the simulation time for at least one of the models/replicas, with values for all models/replicas ranging from 0 to 95%, and with larger variations across models/replicas than across subunits. A somewhat loose geometric definition designed to include weak hydrogen bonds was used, as described in Methods. The cholesterol hydroxyl acts as both donor and acceptor, with various divisions ranging from pure donor to pure acceptor across the subunits and simulations. A

sample configuration illustrating such an H-bond is shown in Fig. S6: the cholesterol headgroup penetrates deep into the bundle. In the γ subunit, however, M2 S15′ did not form an H-bond with cholesterol for >2% of the simulation time in any of the simulations; we note that the corresponding cholesterol molecules in the β-γ interface are those for which the most convergence across simulations was observed.

Persistent hydrogen bonds between the cholesterol and M2 helices could result in a net force contributing to the influence of cholesterol on pore conformation. A hydrogen bond under tension would pull the upper part of the M2 helix outward, acting against pore closure. To probe for such an effect, the force exerted on Ser15′ by H-bonded cholesterol was computed, and its average was found to be a repulsion between 50 and 100 pN (0.8–1.5 kcal/mol/Å) across simulations and subunits. Thus, hydrogen-bonded cholesterol does not pull the M2 helix outward but rather, on average, exerts a force pushing it inward. H-bonding therefore does not constitute a direct mechanism that would explain any reduced pore closure in the presence of bound cholesterol, yet it stabilizes cholesterol in its bound state.

Effect of cholesterol on the ion channel pore

The presence or absence of a ligand in the intersubunit site is expected to affect the width of the cleft, as was noted by Yoluk et al. (34) in simulations of GluCl with and without ivermectin. The authors saw the cleft remain stable in the presence of ligand and shrink slightly in its absence. A similar analysis performed on the trajectories in this study indicates that the cholesterol-bound clefts widen by 1.3 Å, whereas cholesterol-free clefts widen by 0.3 Å on average.

Fig. 4 shows the time evolution of the pore radius profile for all systems. The ring of leucines (thought to function as a hydrophobic gate) occurring at α 264 (M2 9′) consistently forms the most constricted region of the pore. For both models that were simulated (Models 1 and 2) both with and without directly bound cholesterol, the addition of directly bound cholesterol widens the pore in the region z = 0–15 Å, which corresponds to the region closest to the cholesterol hydroxyl. This result is consistent with a wedge-type mechanism for positive modulation, as proposed for ivermectin activation of GluCl in Hibbs and Gouaux (32).

The extent to which this widening of the pore near the cholesterol hydroxyl correlates with widening of the pore at its narrowest constriction (which would seem to be the most influential region for determining conduction) is mixed for the two models, however. Fig. 4 indicates that for Model 1, bound cholesterol clearly widens the narrowest constriction, as evidenced by a marked reduction in black regions in the band formed by M2 9′ (this effect is consistent across the three replicas). In Model 2, however, the constriction at M2 9′ is largely unchanged in the presence of docked cholesterol.

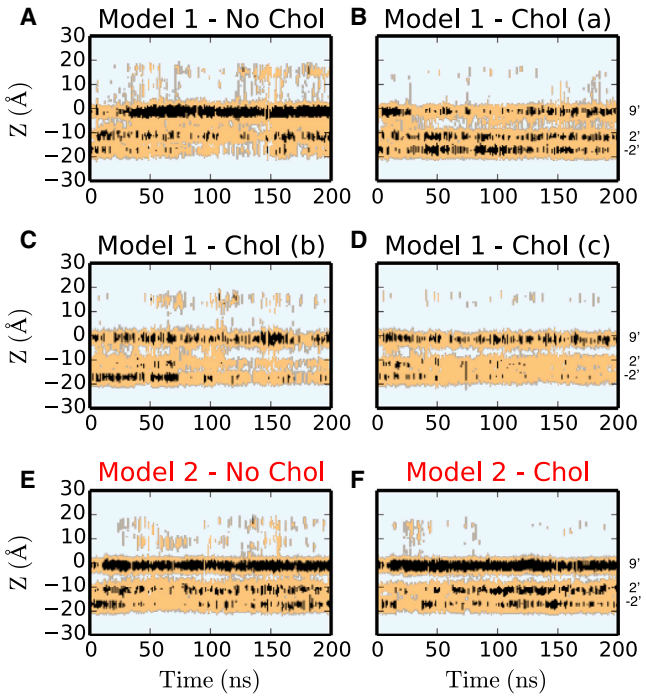

FIGURE 4 Time evolution of the pore radius profile (along the pore axis) for Models 1 (*A–D*) and 2 (*E* and *F*). Pore radii >3 Å, between 2 and 3 Å, and <2 Å are color-coded as light blue, orange, and black, respectively. The prime numbering corresponds to Leu^{264} (9′), Val^{257} (2′) and Pro^{253} (−2′) in the M2 helix of the α subunit. To see this figure in color, go online.

More quantitative analysis can be obtained by defining multiple average geometric parameters of the M2 helices, as represented in Fig. 5. The geometric parameters analyzed are the pore radius, p, at M2 9′; the average distance q between the pore axis and the center of the M2 helix at 9′; the average radial tilt angle, θ, of the M2 half-helix on the extracellular side with respect to the pore axis projected along the radial vector; and the average distance r between the pore axis and the center of the M2 helix at 15′. The latter three parameters are related, on average, by $\langle q \rangle = \langle r \rangle - l_0 \sin\langle\theta\rangle$, where l_0 = 6.4 Å is the distance along the helix between 9′ and 15′. The results from such decomposition indicate that the presence of cholesterol has similar effects on the measured distance r in both Models 1 and 2, although the effect is less pronounced for Model 2. This result is again consistent with a wedge mechanism, in which cholesterol widens the radius of the M2 helices at its point of contact. Furthermore, the difference in distances from the pore axis to the side chain at 9′ and to the helix center at 9′ ($q - p$) is roughly conserved for all six Model 1/Model 2 systems, indicating that effects of cholesterol or model dependence of the pore radius are not determined by rotation of M2 helices or different conformations of side chains in the pore. The difference in cholesterol sensitivity of the two models seems to originate from a higher value of the average tilt angle, θ, in the Model 2 system with cholesterol. The origin of this larger tilt is not clear, but the largest difference in average θ between

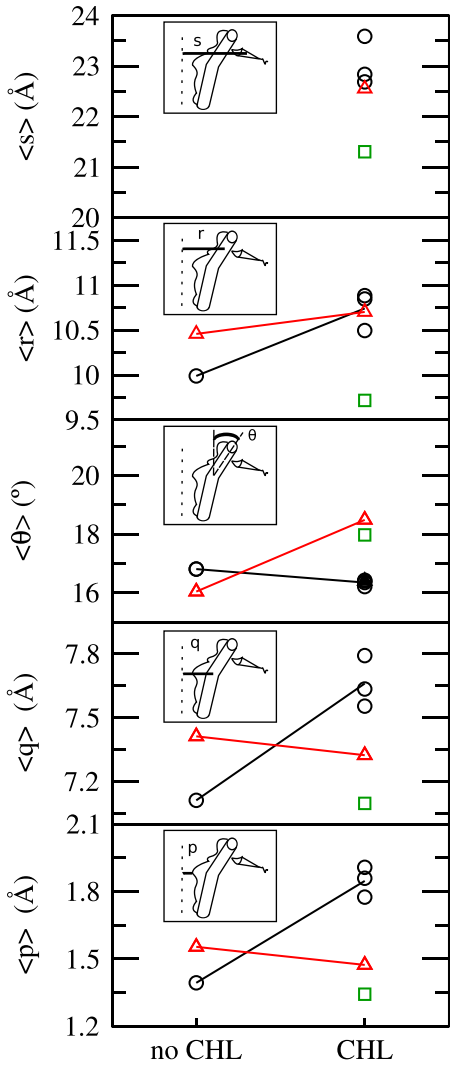

FIGURE 5 Pore geometric properties, averaged over subunits and simulation frames. Definitions for each property are shown in the insets. Data for Model 1 (*black circles*), Model 2 (*red triangles*), and Model 3 (*green square*) are shown. Lines are shown to guide the eye and reflect the implicit hypothesis that trends should be characterized on a per-model basis. The first 50 ns of simulation are not included in these averages. To see this figure in color, go online.

the two models is found in the β subunits; likewise, the salt bridge that is present in β subunits for Model 2 and absent in Model 1 constitutes one of the biggest differences between the two models. The potential key role of these salt bridges has been outlined previously (97), although errors in the then-prevalent Unwin models may have led to inaccurate placement of some of the residues involved.

DISCUSSION

In this work, we investigate the implications of potential cholesterol binding to intersubunit ivermectin/neurosteroid sites on the $GABA_AR$. We build models of a human $GABA_AR$ based on the crystal structure of the glutamate-gated chloride channel of *C. elegans*. The models bring to light putative disulfide bridges linking the M1 and M3 transmembrane helices of the α and γ subunits. Currently available evidence is insufficient to confirm or refute the existence and functional significance of such disulfide bridges; however, sequence analysis shows that the cysteine residues involved are characteristic of the α and γ subunit types across all vertebrate $GABA_ARs$.

Based on structural and biochemical evidence, we postulate a binding mode of cholesterol at the subunit interfaces, analogous to ivermectin binding to the GluCl receptor. We construct bound-cholesterol coordinates by alignment with the ivermectin coordinates of the template. This hypothesis is confirmed independently by automated docking calculations that show pseudosymmetric binding modes overlapping with ivermectin coordinates, although in a slightly different orientation than we initially postulated. In explicit-solvent, atomistic MD simulations, we find that cholesterol is generally stable, but possibly mobile in these sites, with fluctuations between several orientations. In these simulations, we observe instances of spontaneous unbinding and rebinding of cholesterol in poses and orientations similar to those predicted by docking. On the relatively short timescale spanned by our simulations, cholesterol tends to promote pore opening, although that effect is less pronounced in one of the structural models.

Several crystal structures of membrane receptors showing bound cholesterol molecules have been resolved, starting with the β2-adrenergic receptor (98); there is also experimental evidence of direct, specific interactions of cholesterol with membrane channels VDAC (99), KirBac1.1 (100), Kir2 (101), and TRPV1 (102). In general, interactions documented experimentally occur at the lipid interface and describe a transmembrane orientation of cholesterol similar to its bulk bilayer orientation. This model, like our previous model of interaction with the nAChR, depicts a deeper type of binding than do most other models, in between TM helices. Such binding could be very difficult to access experimentally for several reasons, such as slow exchange with bulk on the timescale of experiments. It could also be relatively unusual and limited to few classes of transmembrane proteins.

The direct-interaction model presented here lends itself to experimental testing by mutagenesis. Our bound-cholesterol structural models indicate key residues that are likely to be involved in cholesterol interactions and constitute prime targets for mutagenesis. In addition to M2 Ser15′, already highlighted by biochemical (103) and structural work (32), residues of helices M1 and M3 are predicted to form nonpolar contacts with the steroid nucleus of cholesterol.

Future work will seek to predict the affinity of cholesterol for these sites; at present, we note that vertebrate $GABA_ARs$ reside in cholesterol-rich membranes (36), and that therefore it is likely that at least some of these intersubunit sites

are occupied by cholesterol. Binding of neurosteroids or other modulators may then proceed through exchange between the cholesterol and the modulator rather than opening of an empty, collapsed site.

SUPPORTING MATERIAL

Six figures are available at http://www.biophysj.org/biophysj/supplemental/S0006-3495(14)00324-5.

We thank Dr. Antoine Taly for many fruitful discussions. We also acknowledge use of computational resources from the National Science Foundation XSEDE program through allocation MCB110140, as well as from Centre de Calcul Recherche et Technologie (Bruyères-le-Châtel, France), Centre Informatique National de l'Enseignement Supérieur (Montpellier, France) and Institut du Développement et des Ressources en Informatique (Orsay, France) under allocation 2013-077058 made by Grand Equipement National de Calcul Intensif.

This research was funded by grant MCB1330728 from the National Science Foundation, and grant P01GM55876-14A1 from the National Institutes of Health.

REFERENCES

1. Olsen, R. W., and A. J. Tobin. 1990. Molecular biology of $GABA_A$ receptors. *FASEB J.* 4:1469–1480.
2. Macdonald, R. L., and R. W. Olsen. 1994. $GABA_A$ receptor channels. *Annu. Rev. Neurosci.* 17:569–602.
3. Rabow, L. E., S. J. Russek, and D. H. Farb. 1995. From ion currents to genomic analysis: recent advances in $GABA_A$ receptor research. *Synapse.* 21:189–274.
4. Macdonald, R. L., J.-Q. Kang, …, H.-J. Feng. 2006. $GABA_A$ receptor mutations associated with generalized epilepsies. *Adv. Pharmacol.* 54:147–169.
5. Lewis, D. A., D. W. Volk, and T. Hashimoto. 2004. Selective alterations in prefrontal cortical GABA neurotransmission in schizophrenia: a novel target for the treatment of working memory dysfunction. *Psychopharmacology* (*Berl.*). 174:143–150.
6. Ishikawa, M., K. Mizukami, …, T. Asada. 2004. $GABA_A$ receptor γ subunits in the prefrontal cortex of patients with schizophrenia and bipolar disorder. *Neuroreport.* 15:1809–1812.
7. Lo, W.-S., C.-F. Lau, …, H. Xue. 2004. Association of SNPs and haplotypes in $GABA_A$ receptor $\beta 2$ gene with schizophrenia. *Mol. Psychiatry.* 9:603–608.
8. Rissman, R. A., and W. C. Mobley. 2011. Implications for treatment: $GABA_A$ receptors in aging, Down syndrome and Alzheimer's disease. *J. Neurochem.* 117:613–622.
9. Porjesz, B., L. Almasy, …, H. Begleiter. 2002. Linkage disequilibrium between the β frequency of the human EEG and a $GABA_A$ receptor gene locus. *Proc. Natl. Acad. Sci. USA.* 99:3729–3733.
10. Edenberg, H. J., D. M. Dick, …, H. Begleiter. 2004. Variations in GABRA2, encoding the α 2 subunit of the $GABA_A$ receptor, are associated with alcohol dependence and with brain oscillations. *Am. J. Hum. Genet.* 74:705–714.
11. Krasowski, M. D., and N. L. Harrison. 1999. General anaesthetic actions on ligand-gated ion channels. *Cell. Mol. Life Sci.* 55:1278–1303.
12. Miller, K. W. 2002. The nature of sites of general anaesthetic action. *Br. J. Anaesth.* 89:17–31.
13. Hemmings, Jr., H. C., M. H. Akabas, …, N. L. Harrison. 2005. Emerging molecular mechanisms of general anesthetic action. *Trends Pharmacol. Sci.* 26:503–510.
14. Möhler, H., F. Crestani, and U. Rudolph. 2001. $GABA_A$-receptor subtypes: a new pharmacology. *Curr. Opin. Pharmacol.* 1:22–25.
15. Rudolph, U., and H. Möhler. 2006. GABA-based therapeutic approaches: $GABA_A$ receptor subtype functions. *Curr. Opin. Pharmacol.* 6:18–23.
16. Lambert, J. J., M. A. Cooper, …, D. Belelli. 2009. Neurosteroids: endogenous allosteric modulators of $GABA_A$ receptors. *Psychoneuroendocrinology.* 34 (*Suppl 1*):S48–S58.
17. Mitchell, E. A., M. B. Herd, …, D. Belelli. 2008. Neurosteroid modulation of $GABA_A$ receptors: molecular determinants and significance in health and disease. *Neurochem. Int.* 52:588–595.
18. Belelli, D., and J. J. Lambert. 2005. Neurosteroids: endogenous regulators of the $GABA_A$ receptor. *Nat. Rev. Neurosci.* 6:565–575.
19. Akk, G., D. F. Covey, …, S. Mennerick. 2007. Mechanisms of neurosteroid interactions with $GABA_A$ receptors. *Pharmacol. Ther.* 116:35–57.
20. Miyazawa, A., Y. Fujiyoshi, and N. Unwin. 2003. Structure and gating mechanism of the acetylcholine receptor pore. *Nature.* 423:949–955.
21. Unwin, N. 2005. Refined structure of the nicotinic acetylcholine receptor at 4 Å resolution. *J. Mol. Biol.* 346:967–989.
22. Hilf, R. J. C., and R. Dutzler. 2008. X-ray structure of a prokaryotic pentameric ligand-gated ion channel. *Nature.* 452:375–379.
23. Pan, J., Q. Chen, …, P. Tang. 2012. Structure of the pentameric ligand-gated ion channel ELIC cocrystallized with its competitive antagonist acetylcholine. *Nat. Commun.* 3:714.
24. Hilf, R. J. C., and R. Dutzler. 2009. Structure of a potentially open state of a proton-activated pentameric ligand-gated ion channel. *Nature.* 457:115–118.
25. Bocquet, N., H. Nury, …, P.-J. Corringer. 2009. X-ray structure of a pentameric ligand-gated ion channel in an apparently open conformation. *Nature.* 457:111–114.
26. Hilf, R. J. C., C. Bertozzi, …, R. Dutzler. 2010. Structural basis of open channel block in a prokaryotic pentameric ligand-gated ion channel. *Nat. Struct. Mol. Biol.* 17:1330–1336.
27. Nury, H., C. Van Renterghem, …, P.-J. Corringer. 2011. X-ray structures of general anaesthetics bound to a pentameric ligand-gated ion channel. *Nature.* 469:428–431.
28. Prevost, M. S., L. Sauguet, …, P.-J. Corringer. 2012. A locally closed conformation of a bacterial pentameric proton-gated ion channel. *Nat. Struct. Mol. Biol.* 19:642–649.
29. Corringer, P.-J., F. Poitevin, …, J.-P. Changeux. 2012. Structure and pharmacology of pentameric receptor channels: from bacteria to brain. *Structure.* 20:941–956.
30. Jansen, M., M. Bali, and M. H. Akabas. 2008. Modular design of Cys-loop ligand-gated ion channels: functional 5-HT3 and GABA ρ1 receptors lacking the large cytoplasmic M3M4 loop. *J. Gen. Physiol.* 131:137–146.
31. Dacosta, C. J. B., and J. E. Baenziger. 2013. Gating of pentameric ligand-gated ion channels: structural insights and ambiguities. *Structure.* 21:1271–1283.
32. Hibbs, R. E., and E. Gouaux. 2011. Principles of activation and permeation in an anion-selective Cys-loop receptor. *Nature.* 474: 54–60.
33. Lynagh, T., and J. W. Lynch. 2012. Molecular mechanisms of Cys-loop ion channel receptor modulation by ivermectin. *Front. Mol. Neurosci.* 5:60.
34. Yoluk, O., T. Brömstrup, …, E. Lindahl. 2013. Stabilization of the GluCl ligand-gated ion channel in the presence and absence of ivermectin. *Biophys. J.* 105:640–647.
35. Calimet, N., M. Simoes, …, M. Cecchini. 2013. A gating mechanism of pentameric ligand-gated ion channels. *Proc. Natl. Acad. Sci. USA.* 110:E3987–E3996.
36. North, P., and S. Fleischer. 1983. Alteration of synaptic membrane cholesterol/phospholipid ratio using a lipid transfer protein. Effect on γ-aminobutyric acid uptake. *J. Biol. Chem.* 258:1242–1253.
37. Criado, M., H. Eibl, and F. J. Barrantes. 1982. Effects of lipids on acetylcholine receptor. Essential need of cholesterol for maintenance

of agonist-induced state transitions in lipid vesicles. *Biochemistry.* 21:3622–3629.

38. Dalziel, A. W., E. S. Rollins, and M. G. McNamee. 1980. The effect of cholesterol on agonist-induced flux in reconstituted acetylcholine receptor vesicles. *FEBS Lett.* 122:193–196.
39. Rankin, S. E., G. H. Addona, …, K. W. Miller. 1997. The cholesterol dependence of activation and fast desensitization of the nicotinic acetylcholine receptor. *Biophys. J.* 73:2446–2455.
40. Marsh, D., and F. J. Barrantes. 1978. Immobilized lipid in acetylcholine receptor-rich membranes from *Torpedo marmorata*. *Proc. Natl. Acad. Sci. USA.* 75:4329–4333.
41. Jones, O. T., and M. G. McNamee. 1988. Annular and nonannular binding sites for cholesterol associated with the nicotinic acetylcholine receptor. *Biochemistry.* 27:2364–2374.
42. Leibel, W. S., L. L. Firestone, …, K. W. Miller. 1987. Two pools of cholesterol in acetylcholine receptor-rich membranes from *Torpedo*. *Biochim. Biophys. Acta.* 897:249–260.
43. Gimpl, G., K. Burger, and F. Fahrenholz. 1997. Cholesterol as modulator of receptor function. *Biochemistry.* 36:10959–10974.
44. Fantini, J., and F. J. Barrantes. 2009. Sphingolipid/cholesterol regulation of neurotransmitter receptor conformation and function. *Biochim. Biophys. Acta.* 1788:2345–2361.
45. Barrantes, F. J. 2007. Cholesterol effects on nicotinic acetylcholine receptor. *J. Neurochem.* 103 (*Suppl 1*):72–80.
46. daCosta, C. J. B., A. A. Ogrel, …, J. E. Baenziger. 2002. Lipid-protein interactions at the nicotinic acetylcholine receptor. A functional coupling between nicotinic receptors and phosphatidic acid-containing lipid bilayers. *J. Biol. Chem.* 277:201–208.
47. daCosta, C. J. B., and J. E. Baenziger. 2009. A lipid-dependent uncoupled conformation of the acetylcholine receptor. *J. Biol. Chem.* 284:17819–17825.
48. Zabrecky, J. R., and M. A. Raftery. 1985. The role of lipids in the function of the acetylcholine receptor. *J. Recept. Res.* 5:397–417.
49. Lechleiter, J., M. Wells, and R. Gruener. 1986. Halothane-induced changes in acetylcholine receptor channel kinetics are attenuated by cholesterol. *Biochim. Biophys. Acta.* 856:640–645.
50. Santiago, J., G. R. Guzmàn, …, J. A. Lasalde-Dominicci. 2001. Probing the effects of membrane cholesterol in the *Torpedo californica* acetylcholine receptor and the novel lipid-exposed mutation α C418W in *Xenopus* oocytes. *J. Biol. Chem.* 276:46523–46532.
51. Borroni, V., C. J. Baier, …, F. J. Barrantes. 2007. Cholesterol depletion activates rapid internalization of submicron-sized acetylcholine receptor domains at the cell membrane. *Mol. Membr. Biol.* 24:1–15.
52. Báez-Pagán, C. A., Y. Martínez-Ortiz, …, J. A. Lasalde-Dominicci. 2008. Potential role of caveolin-1-positive domains in the regulation of the acetylcholine receptor's activatable pool: implications in the pathogenesis of a novel congenital myasthenic syndrome. *Channels (Austin).* 2:180–190.
53. daCosta, C. J. B., L. Dey, …, J. E. Baenziger. 2013. A distinct mechanism for activating uncoupled nicotinic acetylcholine receptors. *Nat. Chem. Biol.* 9:701–707.
54. Brannigan, G., J. Hénin, …, M. L. Klein. 2008. Embedded cholesterol in the nicotinic acetylcholine receptor. *Proc. Natl. Acad. Sci. USA.* 105:14418–14423.
55. Cheng, M. H., Y. Xu, and P. Tang. 2009. Anionic lipid and cholesterol interactions with $\alpha 4\beta 2$ nAChR: insights from MD simulations. *J. Phys. Chem. B.* 113:6964–6970.
56. Bristow, D. R., and I. L. Martin. 1987. Solubilisation of the γ-aminobutyric acid/benzodiazepine receptor from rat cerebellum: optimal preservation of the modulatory responses by natural brain lipids. *J. Neurochem.* 49:1386–1393.
57. Dunn, S. M., C. R. Martin, …, R. Miyazaki. 1989. Functional reconstitution of the bovine brain GABAA receptor from solubilized components. *Biochemistry.* 28:2545–2551.
58. Sooksawate, T., and M. A. Simmonds. 2001. Effects of membrane cholesterol on the sensitivity of the $GABA_A$ receptor to GABA in acutely dissociated rat hippocampal neurones. *Neuropharmacology.* 40:178–184.
59. Chisari, M., L. N. Eisenman, …, C. F. Zorumski. 2010. The sticky issue of neurosteroids and $GABA_A$ receptors. *Trends Neurosci.* 33:299–306.
60. Covey, D. F., A. S. Evers, …, R. H. Purdy. 2001. Recent developments in structure-activity relationships for steroid modulators of $GABA_A$ receptors. *Brain Res. Brain Res. Rev.* 37:91–97.
61. Hosie, A. M., M. E. Wilkins, …, T. G. Smart. 2006. Endogenous neurosteroids regulate $GABA_A$ receptors through two discrete transmembrane sites. *Nature.* 444:486–489.
62. Hosie, A. M., M. E. Wilkins, and T. G. Smart. 2007. Neurosteroid binding sites on $GABA_A$ receptors. *Pharmacol. Ther.* 116:7–19.
63. Li, G.-D., D. C. Chiara, …, R. W. Olsen. 2009. Neurosteroids allosterically modulate binding of the anesthetic etomidate to γ-aminobutyric acid type A receptors. *J. Biol. Chem.* 284:11771–11775. http://dx.doi.org/10.1074/jbc.C900016200.
64. Sooksawate, T., and M. A. Simmonds. 2001. Influence of membrane cholesterol on modulation of the $GABA_A$ receptor by neuroactive steroids and other potentiators. *Br. J. Pharmacol.* 134:1303–1311.
65. Krůsek, J., and H. Zemková. 1994. Effect of ivermectin on γ-aminobutyric acid-induced chloride currents in mouse hippocampal embryonic neurones. *Eur. J. Pharmacol.* 259:121–128.
66. Dawson, G. R., K. A. Wafford, …, R. M. McKernan. 2000. Anticonvulsant and adverse effects of avermectin analogs in mice are mediated through the γ-aminobutyric $acid_A$ receptor. *J. Pharmacol. Exp. Ther.* 295:1051–1060.
67. Adelsberger, H., A. Lepier, and J. Dudel. 2000. Activation of rat recombinant $\alpha_1\beta_2\gamma_{2S}$ $GABA_A$ receptor by the insecticide ivermectin. *Eur. J. Pharmacol.* 394:163–170.
68. Tasneem, A., L. M. Iyer, …, L. Aravind. 2005. Identification of the prokaryotic ligand-gated ion channels and their implications for the mechanisms and origins of animal Cys-loop ion channels. *Genome Biol.* 6:R4.
69. Rendon, G., M. R. Kantorovitz, …, E. Jakobsson. 2011. Identifying bacterial and archaeal homologs of pentameric ligand-gated ion channel (pLGIC) family using domain-based and alignment-based approaches. *Channels (Austin).* 5:325–343.
70. Bergmann, R., K. Kongsbak, …, T. Balle. 2013. A unified model of the $GABA_A$ receptor comprising agonist and benzodiazepine binding sites. *PLoS ONE.* 8:e52323.
71. Bertaccini, E. J., O. Yoluk, …, J. R. Trudell. 2013. Assessment of homology templates and an anesthetic binding site within the γ-aminobutyric acid receptor. *Anesthesiology.* 119:1087–1095. http://dx.doi.org/10.1097/ALN.0b013e31829e47e3.
72. Eswar, N., B. Webb, …, A. Sali. 2007. Comparative protein structure modeling using Modeller. *Curr. Protoc. Bioinformatics.* Chapter 5: Unit 5.6.
73. Schreiner, E., L. G. Trabuco, …, K. Schulten. 2011. Stereochemical errors and their implications for molecular dynamics simulations. *BMC Bioinformatics.* 12:190.
74. Humphrey, W., A. Dalke, and K. Schulten. 1996. VMD: visual molecular dynamics. *J. Mol. Graph.* 14:33–38, 27–28.
75. Krivov, G. G., M. V. Shapovalov, and R. L. Dunbrack, Jr. 2009. Improved prediction of protein side-chain conformations with SCWRL4. *Proteins.* 77:778–795.
76. Chen, Q., M. H. Cheng, …, P. Tang. 2010. Anesthetic binding in a pentameric ligand-gated ion channel: GLIC. *Biophys. J.* 99:1801–1809.
77. Trott, O., and A. J. Olson. 2010. AutoDock Vina: improving the speed and accuracy of docking with a new scoring function, efficient optimization, and multithreading. *J. Comput. Chem.* 31:455–461.
78. Pettersen, E. F., T. D. Goddard, …, T. E. Ferrin. 2004. UCSF Chimera—a visualization system for exploratory research and analysis. *J. Comput. Chem.* 25:1605–1612.

79. Jo, S., J. B. Lim, …, W. Im. 2009. CHARMM-GUI Membrane Builder for mixed bilayers and its application to yeast membranes. *Biophys. J.* 97:50–58.

80. MacKerell, Jr., A. D., D. Bashford, …, M. Karplus. 1998. All-atom empirical potential for molecular modeling and dynamics studies of proteins. *J. Phys. Chem. B.* 102:3586–3616.

81. MacKerell, Jr., A. D., M. Feig, and C. L. Brooks, 3rd. 2004. Improved treatment of the protein backbone in empirical force fields. *J. Am. Chem. Soc.* 126:698–699.

82. Klauda, J. B., R. M. Venable, …, R. W. Pastor. 2010. Update of the CHARMM all-atom additive force field for lipids: validation on six lipid types. *J. Phys. Chem. B.* 114:7830–7843.

83. Pitman, M. C., F. Suits, …, S. E. Feller. 2004. Molecular-level organization of saturated and polyunsaturated fatty acids in a phosphatidylcholine bilayer containing cholesterol. *Biochemistry.* 43: 15318–15328.

84. Lim, J. B., B. Rogaski, and J. B. Klauda. 2012. Update of the cholesterol force field parameters in CHARMM. *J. Phys. Chem. B.* 116: 203–210.

85. Phillips, J. C., R. Braun, …, K. Schulten. 2005. Scalable molecular dynamics with NAMD. *J. Comput. Chem.* 26:1781–1802.

86. Essman, U., L. Perela, …, L. G. Pedersen. 1995. A smooth particle mesh Ewald method. *J. Chem. Phys.* 103:8577–8592.

87. Smart, O. S., J. G. Neduvelil, …, M. S. Sansom. 1996. HOLE: a program for the analysis of the pore dimensions of ion channel structural models. *J. Mol. Graph.* 14:354–360, 376.

88. Mnatsakanyan, N., and M. Jansen. 2013. Experimental determination of the vertical alignment between the second and third transmembrane segments of muscle nicotinic acetylcholine receptors. *J. Neurochem.* 125:843–854.

89. Bera, A. K., and M. H. Akabas. 2005. Spontaneous thermal motion of the $GABA_A$ receptor M2 channel-lining segments. *J. Biol. Chem.* 280:35506–35512.

90. Jansen, M., and M. H. Akabas. 2006. State-dependent cross-linking of the M2 and M3 segments: functional basis for the alignment of $GABA_A$ and acetylcholine receptor M3 segments. *J. Neurosci.* 26:4492–4499.

91. Bali, M., M. Jansen, and M. H. Akabas. 2009. GABA-induced intersubunit conformational movement in the $GABA_A$ receptor α1M1-β2M3 transmembrane subunit interface: experimental basis for homology modeling of an intravenous anesthetic binding site. *J. Neurosci.* 29:3083–3092.

92. Bali, M., and M. H. Akabas. 2012. Gating-induced conformational rearrangement of the γ-aminobutyric acid type A receptor β-α subunit interface in the membrane-spanning domain. *J. Biol. Chem.* 287:27762–27770.

93. Marsh, D., A. Watts, and F. J. Barrantes. 1981. Phospholipid chain immobilization and steroid rotational immobilization in acetylcholine receptor-rich membranes from *Torpedo marmorata*. *Biochim. Biophys. Acta.* 645:97–101.

94. Shan, Q., J. L. Haddrill, and J. W. Lynch. 2001. Ivermectin, an unconventional agonist of the glycine receptor chloride channel. *J. Biol. Chem.* 276:12556–12564.

95. Lynagh, T., T. I. Webb, …, J. W. Lynch. 2011. Molecular determinants of ivermectin sensitivity at the glycine receptor chloride channel. *J. Biol. Chem.* 286:43913–43924.

96. Lynagh, T., and J. W. Lynch. 2012. Ivermectin binding sites in human and invertebrate Cys-loop receptors. *Trends Pharmacol. Sci.* 33: 432–441.

97. Law, R. J., and F. C. Lightstone. 2009. Modeling neuronal nicotinic and GABA receptors: important interface salt-links and protein dynamics. *Biophys. J.* 97:1586–1594.

98. Hanson, M. A., V. Cherezov, …, R. C. Stevens. 2008. A specific cholesterol binding site is established by the 2.8 Å structure of the human β2-adrenergic receptor. *Structure.* 16:897–905.

99. Hiller, S., R. G. Garces, …, G. Wagner. 2008. Solution structure of the integral human membrane protein VDAC-1 in detergent micelles. *Science.* 321:1206–1210.

100. Singh, D. K., T.-P. Shentu, …, I. Levitan. 2011. Cholesterol regulates prokaryotic Kir channel by direct binding to channel protein. *Biochim. Biophys. Acta.* 1808:2527–2533.

101. Rosenhouse-Dantsker, A., S. Noskov, …, I. Levitan. 2013. Identification of novel cholesterol-binding regions in Kir2 channels. *J. Biol. Chem.* 288:31154–31164. http://dx.doi.org/10.1074/jbc.M113.496117.

102. Picazo-Juárez, G., S. Romero-Suárez, …, T. Rosenbaum. 2011. Identification of a binding motif in the S5 helix that confers cholesterol sensitivity to the TRPV1 ion channel. *J. Biol. Chem.* 286:24966–24976. http://dx.doi.org/10.1074/jbc.M111.237537.

103. Miller, P. S., and T. G. Smart. 2010. Binding, activation and modulation of Cys-loop receptors. *Trends Pharmacol. Sci.* 31:161–174.